Original Article

MOLECULAR METABOLISM

ISX-9 manipulates endocrine progenitor fate revealing conserved intestinal lineages in mouse and human organoids

Anastasia Tsakmaki [1,4], Patricia Fonseca Pedro [1,4], Polychronis Pavlidis [2], Bu'Hussain Hayee [3], Gavin A. Bewick [1,*]

ABSTRACT

Objective: Enteroendocrine cells (EECs) survey the gut luminal environment and coordinate hormonal, immune and neuronal responses to it. They exhibit well-characterised physiological roles ranging from the control of local gut function to whole body metabolism, but little is known regarding the regulatory networks controlling their differentiation, especially in the human gut. The small molecule isoxazole-9 (ISX-9) has been shown to stimulate neuronal and pancreatic beta-cell differentiation, both closely related to EEC differentiation. Our aim was to use ISX-9 as a tool to explore EEC differentiation.

Methods: We investigated the effects of ISX-9 on EEC differentiation in mouse and human intestinal organoids, using real-time quantitative polymerase chain reaction (RT-qPCR), fluorescent-activated cell sorting, immunostaining and single-cell RNA sequencing.

Results: ISX-9 increased the number of neurogenin3-RFP (Ngn3)-positive endocrine progenitor cells and upregulated NeuroD1 and Pax4, transcription factors that play roles in mouse EEC specification. Single-cell analysis showed induction of Pax4 expression in a developmentally late Ngn3+ population of cells and potentiation of genes associated with progenitors biased toward serotonin-producing enterochromaffin (EC) cells. Further, we observed enrichment of organoids with functional EC cells that was partly dependent on stimulation of calcium signalling in a population of cells residing outside the crypt base. Inducible Pax4 overexpression, in ileal organoids, uncovered its importance as a component of early human endocrine specification and highlighted the potential existence of two major endocrine lineages, the early appearing enterochromaffin lineage and the later developing peptidergic lineage which contains classical gut hormone cell types.

Conclusion: Our data provide proof-of-concept for the controlled manipulation of specific endocrine lineages with small molecules, whilst also shedding new light on human EEC differentiation and its similarity to the mouse. Given their diverse roles, understanding endocrine lineage plasticity and its control could have multiple therapeutic implications.

Keywords Intestinal organoids; Enteroendocrine cells; Gut hormone; Differentiation; Isoxazole; Enterochromaffin cells

1. INTRODUCTION

The intestinal epithelium is a key interface with our external environment. It renews itself every 4–5 days, and is composed of five terminally differentiated cell types: the absorptive enterocytes and the secretory Paneth, goblet, tuft and enteroendocrine cells (EECs) [1]. These cells are constitutively generated by cycling $Lgr5^{+}$ crypt stem cells, and together they orchestrate the epithelium's major functions, nutrient absorption and defence. Despite representing only 1% of the epithelium, the EECs constitute the largest hormone-producing tissue and have been described as the gut's sentinels. They sample the luminal, circulating and local tissue environments and coordinate an appropriate response from the epithelium and the immune and nervous systems [2]. For example, they play a key role in controlling the response to a meal, fine tuning physiology to ensure optimal fuel absorption, use and storage [3]. Gut hormones exhibit actions ranging from the local control of gut motility, absorption and secretion, to the regulation of whole-body metabolism [4]. Whilst there is a large body of evidence describing the functional roles of gut hormones, comparatively little is known about the factors that control EEC differentiation and assign subset identity.

EECs were originally classified by immunostaining according to their dominant hormone product. Glucagon-like peptide 1 (GLP-1), glucagon-like peptide 2 (GLP-2) and peptide YY (PYY) are secreted by L cells; glucose-dependent insulinotrophic polypeptide (GIP) is secreted by K cells; somatostatin (SST) is secreted by D cells; cholecystokinin (CCK) is secreted by I cells; secretin (SCT) is secreted by S cells; gastrin (GAST) is secreted by G cells; serotonin is secreted by enterochromaffin (EC) cells;

[1]Diabetes Research Group, School of Life Course Sciences, Faculty of Life Science and Medicine, King's College London, London, UK [2]Centre for Inflammation Biology and Cancer Immunology, King's College London, London, UK [3]Department of Gastroenterology, King's College Hospital NHS Foundation Trust, London, UK

[4] Anastasia Tsakmaki and Patricia Fonseca Pedro contributed equally to this work.

*Corresponding author. E-mail: gavin.bewick@kcl.ac.uk (G.A. Bewick).

Received November 11, 2019 • Revision received January 8, 2020 • Accepted January 21, 2020 • Available online 17 February 2020

https://doi.org/10.1016/j.molmet.2020.01.012

and neurotensin (NTS) is secreted by N cells. The recent use of fluorescent reporter mice and transcriptomics has showed that EEC subsets may be less well defined [5–8]. The hormonal repertoire of an EEC is a function of its differentiation trajectory, its location within the gut and its height in the crypt–villus axis, which dictates differential exposure to Wnt and bone morphogenic protein (BMP) signalling gradients [9,10]. Mouse lineage tracing studies have identified a handful of transcription factors (TFs) regulating EEC differentiation. Cells exiting the stem cell compartment are fated to be secretory cells by *Notch* inhibition, followed by *Atoh1* expression [11–13]. Atoh^{+} cells are then designated to the endocrine lineage by expression of the bHLH TF neurogenin3 (*Ngn3*) [14,15]. In mice, TFs downstream of *Ngn3* known to be necessary for subset specification include *Insm1* (substance P and NTS) [16], neurogenic differentiation 1 (*NeuroD1*) (SCT and CCK) [17–19], *Nkx2.2* (CCK, GAST, GIP and SST) [20], *Pax4* (5-HT, SCT, GIP, PYY and CCK) [21] *Pax6*, *Foxa1* and *Foxa2* (preproglucagon and its products GLP-1 and 2) [22], *Arx* (GLP-1, GIP, CCK, SCT, GAST and GHRL) [21], and *Lmx1A* (5-HT) [23]. Nevertheless, the regulatory networks controlling EEC identity have remained largely unknown, until a recent sophisticated study described a time-resolved transcriptional road map of mouse EEC fate trajectories [24]. It now appears that classical TFs are more promiscuous than lineage tracing implied. Furthermore, there is a paucity of knowledge regarding EEC specification in human intestinal epithelium due to lack of tractable model systems, although several of the classical TFs are upregulated in response to a *NGN3* pulse in intestinal organoids derived from human pluripotent stem cells [25,26]. Understanding the factors that control gut endocrine pedigree has implications for several clinical conditions including diabetes, obesity, gut inflammatory disorders and perhaps cognitive disorders including depression and anxiety. Deciphering how to manipulate EECs may open novel treatment avenues and offer a clearer understanding of epithelial homeostasis.

To identify a candidate molecule that might influence EEC fate, we drew parallels from other endocrine tissues. Gut endocrine specification is strikingly like that in the pancreas, and both bear close resemblance to neuronal differentiation. The small molecule isoxazole-9 (ISX-9) [*N*-cyclopropyl-5-(thiophen-2-yl)isoxazole-3-carboxamide] was uncovered in a chemical screen for drivers of neuronal differentiation [27]. It activates *NeuroD1* and has also been used to investigate pancreatic beta-cell differentiation [28,29]. We explored the effects of ISX-9 on EEC identity in organoids derived from mouse and human tissue resident stem cells. Our data demonstrate proof-of-concept that specific EEC populations can be manipulated with a small molecule, highlight the similarities between mouse and human EEC differentiation and provide a tool to study human EC cells *in vitro.*

2. MATERIAL AND METHODS

2.1. Mice

In this study, intestinal crypts were isolated from 8- to 12-week-old male C57BL/6 mice. The mice were obtained from Envigo (Bicester UK) and were maintained in cages under controlled temperature (21 °C–23 °C) and light (12 h light/12 h dark) with ad libitum access to food and water. Intestinal tissues from the following transgenic animals were also obtained for the generation of small intestinal organoids: Ngn3-RFP mice [30], *Tg(Neurog3-cre)C1Able/J*::*R26-loxSTOPlox-tdRFP* (Ngn3-Cre-RFP-) mice [31] and *CCK-iCre*::*R26-loxSTOPlox-eYFP* (CCK-Cre-Rosa-eYFP) mice [32].

2.2. Crypt isolation and mouse intestinal organoid culture

Mouse small intestines were harvested and cleaned with cold phosphate-buffered saline (PBS) and separated into two parts: duodenum (proximal 5 cm), and jejunum and ileum. For our experiments, organoids were generated only from the jejenum/ileum part. This part was cut longitudinally, and villi were scraped with a glass slide. The tissue was cut with scissors into 2x2-mm pieces and repeatedly washed. Subsequently, the tissue pieces were incubated with 2 mM ethylenediamine tetraacetic acid (EDTA; Invitrogen) in PBS for 45 min in a rotator at 4 °C. After removal of EDTA, vigorous shaking in cold PBS lead to the release of crypts. The crypts were further washed in PBS, passed through a 40-μm cell strainer, pelleted and resuspended in basal medium Eagle (BME; Amsbio). The crypts were plated in 48-well plates, with 200 crypts per 25 μL of BME. The BME was polymerised for 15 min at 37 °C, and stem cell growth medium (WENR) supplemented with 10 μM Y-27632 (Sigma–Aldrich) was overlaid. WENR medium consists of advanced Dulbecco modified Eagle medium (DMEM)/F12, 2 mM GlutaMAX, 10 mM HEPES, 100 units/mL penicillin/streptomycin, 50 ng/mL EGF, 1× B27, 1× N2 supplements (all from Gibco), 1.25 mM N-acetylcysteine (Sigma–Aldrich), 100 ng/mL Noggin (Peprotech), 50% Wnt3A conditioned medium and 10% R-spondin-1 conditioned medium (both in house production). Three days later, the medium was changed into differentiation media (ENR) with no Wnt3A or Y-27632. Organoids were passaged once a week by mechanical dissociation, at a 1:3 split ratio. Plated organoids were maintained in a CO_2 incubator with 5% CO_2, and the media were changed every other day.

The treatment of mouse small intestine organoids with ISX-9 (Tocris Bioscience) started 3 days after passaging. For dose–response experiments, organoids were treated with 2 μM, 20 μM, 40 μM and 80 μM ISX-9 for 48 h. For time-course experiments, organoids were treated with 40 μM ISX-9 for 24, 48 and 96 h, and samples were collected for RNA extraction at the end of each timepoint. Treatment with 10 μM KN93 or 10 μM KN92 (an inactive analogue of KN93) (Tocris Bioscience) in the presence or absence of ISX-9 was also performed for 48 h. For the remaining experiments, organoids were treated with 40 μM ISX-9 for 48 h, and then ISX-9 was removed for another 48 h (48-h ISX-9 pulse).

2.3. Generation and culture of human terminal ileal organoids

Human terminal ileum crypts were isolated from biopsies acquired from patients undergoing colonoscopy at Guy's and St. Thomas's NHS Foundation Trust with their informed consent. Biopsies were washed in cold PBS until the supernatant was clear. Following 10 min of incubation at room temperature with 10 mM 1,4-dithiothreitol (DTT), the biopsies were incubated with 8 mM EDTA in PBS and placed in a rotator for 1 h at 4 °C. At the end of the incubation, the EDTA was removed and crypts were released with vigorous shaking in cold PBS. The crypts were further washed in PBS, pelleted and resuspended in Matrigel (Corning), in the same density as mouse crypts. Human intestinal crypts embedded in Matrigel were overlaid with stem cell growth medium (WENRAS) supplemented with 10 μM Y-27632 and 5 μM CHIR99021 (Sigma–Aldrich). The human stem cell growth medium, in addition to the components of the previously described mouse medium, also contained 10 nM gastrin (Sigma–Aldrich), 500 nM A83-01 (Bio-techne), 10 μM SB202190 (Sigma–Aldrich) and 10 mM nicotinamide (Sigma–Aldrich). Three days after isolation or splitting, Y-27632 and CHIR99221 were removed from the medium, and organoids were either maintained in WENRAS or transferred into differentiation medium for setting up experiments. For the differentiation of human ileal organoids, Wnt3A conditioned medium was reduced from 50% to 15%, and SB202190 and nicotinamide were withdrawn from the medium. Differentiation medium was used for 7 days, keeping the organoids in culture for 10 days. Five days after

passaging, human terminal ileal organoids were treated with 40 μM ISX-9 for 48 h, and then ISX-9 was removed for another 48 h (48-h ISX-9 pulse), except if it is stated differently. MEK signalling was inhibited with 500 nM PD0325901 (Sigma—Aldrich), and notch signalling was inhibited with 10 μM diaminophenylthiazole (DAPT; Sigma—Aldrich). A combination of both inhibitors with ISX-9 was given in a 48-hour pulse. All control organoids were treated with vehicle.

2.4. RNA extraction and real-time quantitative PCR

Total RNA was isolated from organoids [released from Matrigel or BME with Cell Recovery solution (Corning)] using the RNeasy Mini Kit (Qiagen) according to the manufacturer's instructions. On-column DNase digestion was performed for removing any residual genomic DNA (Qiagen). RNA extraction from sorted cells was performed using TRI Reagent LS (Sigma—Aldrich) according to the manufacturer's instruction. cDNA was generated using the High-Capacity cDNA reverse Transcription Kit (Applied Biosystems). Real-time quantitative polymerase chain reaction (RT-qPCR) was performed using QuantiTect primers and QuantiFast SybrGreen PCR kit (both from Qiagen) on a LightCycler 480 or LightCycler 96 (Roche). The relative gene expression levels were calculated by averaging the Ct values of technical duplicates for each biological sample and normalising them to the expression of the housekeeping gene beta-2-microglobulin.

2.5. Evaluation of mouse small intestinal organoid growth

Growth and convolutedness of organoids were evaluated by collecting brightfield images of control and ISX-9-treated organoids with the EOS 600D Nikon camera on an TMS-inverted microscope (Nikon) on days 3, 5 and 7 in culture. The surface area, perimeter and number of buds were measured using ImageJ software.

2.6. Immunofluorescent staining of organoids

Mouse or human small intestine organoids were fixed for 45 min in 4% formalin (Sigma—Aldrich) and then washed with 2% bovine serum albumin (BSA) in PBS (Sigma—Aldrich). Subsequently, organoids were blocked with blocking buffer consisting of 2% BSA and 5% donkey serum (Sigma—Aldrich), and permeabilised with 0.5% Triton-X (Sigma—Aldrich) for 1 h at room temperature. Primary antibody incubation was done in a rotor overnight at 4 °C with primary antibodies diluted in blocking buffer. The primary antibodies used were rabbit polyclonal anti-Chromogranin A (1:800; Abcam) and goat polyclonal anti-serotonin (1:100; Immunostar). The next day, the organoids were washed and incubated with secondary antibodies, Alexa Fluor 488 Donkey Anti-Rabbit or Alexa Fluor 594-Donkey anti-goat (1:500; Jackson ImmunoResearch) for 1 h at room temperature. Nuclear counterstaining was performed in parallel with the secondary antibody incubation using Hoechst 33342 (1:2000; Invitrogen). After washing, organoids were mounted with Vectashield Vibrance Antifade Mounting Medium (Vector Laboratories).

The fraction of proliferating cells in control and ISX-9-treated mouse intestinal organoids was determined using the Click-iT EdU Cell proliferation kit, Alexa Fluor™ 647 dye (Invitrogen). Organoids were pre-incubated for 1 h with 10 μM EdU, then fixed and permeabilised, and EdU-positive nuclei were labelled according to the manufacturer's instructions.

2.7. Immunofluorescent imaging

Live-cell fluorescence imaging was conducted in control and ISX-9-treated Ngn3-RFP, Ngn3-Cre-RFP, and CCK-Cre-Rosa-eYFP organoids. A continuous z dimension stack of RFP or eYFP fluorescence and brightfield images was obtained, while organoids were still embedded on BME, using an A1 inverted confocal microscope (Nikon). Images of whole-mount organoids stained for chromogranin A and serotonin were also captured with an A1 inverted confocal microscope (Nikon). Image analysis was performed using either Nikon Elements or Image J software. Time-lapse fluorescent microscopy of doxycycline-induced human intestinal organoids for overexpression of *Pax4* was performed with a BioStation IM-Q (Nikon).

2.8. Flow cytometry analysis and fluorescence-activated cell sorting (FACS)

Control and ISX-9-treated Ngn3-RFP, Ngn3-Cre-RFP and CCK-Cre-Rosa-eYFP organoids were dissociated into single cells with mechanical disruption after a 5-minute incubation with TrypLE Express (Gibco) at 37 °C. After washing with PBS, the cells were passed through a 40-μm cell strainer and resuspended in Advanced DMEM/F12 medium with 4 μg/mL DNase (Sigma—Aldrich), 10 μM Y-27632 and 2 mM EDTA. Next, 1 μg/mL 4,6-diamino-2-phenylindole (DAPI; Invitrogen) was added to the cell suspension to label dead cells. Viable cells were analysed in a BD FACS Canto™ II (Beckton Dickinson). For RNA extraction of $Ngn3^{+}$ cells from control and ISX-9-treated Ngn3-Cre-RFP organoids, organoids were first dissociated into single cells as previously described and immediately sorted using a BD FACS Aria™ II (Beckton Dickinson).

2.9. Sample preparation for scRNA-seq

Ngn3-Cre-RFP organoids were treated with ISX-9 for 48 h, collected and processed for fluorescence-activated cell sorting as just described. DAPI was added immediately before sorting. RFP-positive, DAPI-negative cells were sorted into 384-well plates containing 384 unique molecular identifier (UMI) barcode primer-sets using a FACS Aria™ II (Beckton Dickinson). Samples in plates were centrifuged and stored at −80 °C. The samples were then processed by Single Cell Discoveries B.V. according the SORT-seq method [33]. Briefly, first and second strand synthesis (Invitrogen) was performed and all wells of a single plate were pooled. After *in vitro* transcription (Ambion), the amplified RNA was reverse transcribed and amplified for 10 to 12 cycles with Illumina Truseq primers. Finally, libraries were analysed on an Illumina NextSeq500 using 75-bp pair-end sequencing.

2.10. Analysis single-cell mRNA sequencing

UMI count matrices were imported into R Studio and processed with the R package Seurat (version 3.1) [34]. For quality control (QC), we quantified the proportions of UMIs mapped to the mitochondrial genome. All the cells with mitochondrial reads greater than 10% were excluded. We further filtered cells with greater than 7500 unique features, and 206 control and 216 ISX cells were passed to analysis. ERCC92 spike-ins as well as genes associated with clustering artefacts (Rn45s, Malat1, Kcnq1ot1, A630089N07Rik) were also excluded from the final dataset. Control and treated datasets were merged after QC filtering and then split by treatment for normalisation using the SCTransform wrapper and percent mitochondrial variations regressed. We calculated a subset of 3000 features to integrate using the SelectIntegrationFeatures and ensured all Pearson residuals were calculated using PrepSCTIntegration. The datasets were then integrated using the FindIntegrationAnchors and the IntegrateData functions. We then ran an integrated analysis on all cells in the experiment using the standard workflow with the following default parameters: linear dimensional reduction using RunPCA, non-linear dimensional reduction using RunUMAP. A K-nearest neighbour's graph was constructed with the FindNeighbors function using the first 25 principle components before clustering using the FindClusters function with a

resolution of 1.8. Differential gene analysis for cluster definition was run using the FindConservedMarkers, which reports the top markers conserved between the control and treated groups. The single-cell FASTQ and read count files are available in the GEO database (accession no. GSE143221).

2.11. Serotonin release from mouse and human small intestine organoids

Serotonin secretion in control and ISX-9-treated mouse organoids was measured after 7 days in culture and in human organoids after 10 days in culture. A 48-hour ISX-9 pulse was given to both mouse and human organoids as just described. At the end of the culture period, organoids were released from BME and Matrigel with Cell Recovery solution (Corning), washed with PBS and incubated with *N*-2-hydroxyethylpiperazine-*N*-2-ethanesulfonic acid (HEPES) saline buffer [of 4.5 mM KCl, 138 mM NaCl, 4.2 mM $NaHCO_3$, 1.2 mM $NaH_2PO_4 \cdot 2H_2O$, 2.6 mM $CaCl_2$, 1.2 mM $MgCl_2$ and 10 mM HEPES (pH 7.4)] with 0.5% BSA for 2 h. Serotonin secretion was stimulated with 10 μM IBMX (Sigma—Aldrich) and 10 μM Forskolin (Sigma—Aldrich) in the presence of 1 μM fluoxetine (Sigma—Aldrich) for blocking potential serotonin reuptake via serotonin transporter (SERT) for 1 h. Supernatant and organoid lysates were collected for measuring secretion and content, respectively. Organoid lysates were prepared in 1× PBS with protease inhibitors (Thermo Scientific). Lysates were frozen at −20 °C, thawed and sonicated for 30 s (amplitude 10—14) on ice, and centrifuged for 5 min at 5000 g at 4 °C. Serotonin concentration was measured using an enzyme-linked immunosorbent assay (ELISA) kit according to the manufacturer's instructions (Aviva System Biology).

2.12. Calcium imaging

Petri dishes (30 mm) were coated with BME diluted in Advanced DMEM/F12 (1:100) and left to set at 37 °C for 1 h. Mouse small intestine organoids were collected and washed three times with cold PBS to dissolve BME and re-seeded in BME-coated Petri dishes with ENR medium. After 2 h, organoids were loaded with 7 μM Fura 2-AM (Sigma—Aldrich) in HEPES saline buffer containing 0.01% pluronic F127 (Invitrogen) and 2 mM probenecid (Tocris Bioscience), and incubated for 30 min at 37 °C. Organoids were washed three times with HEPES buffer, and images were recorded with an Axiovert 135 Ca^{2+} imaging system (Zeiss), at 20× magnification every 80 ms. Cells were excited at 340 nm and 380 nm, and emitted light was acquired at 510 nm. Calcium concentration was calculated by 340/380 fluorescence ratio using MetaFluor software. Adenosine triphosphate (ATP; 100 μM) was used as positive control. Imaging experiments were performed at least three times, and the representative time course is presented in the manuscript.

2.13. Genetic engineering of human terminal ileal organoids

For overexpression of *Pax4* in human terminal ileal organoids, mouse *Pax4* cDNA was cloned into the pPB-tetO-MCS-IRES-mCherry vector. Briefly, pPB-tetO-MCS-IRES-mCherry vector was first linearised following sequential digestion with XhoI and SpeI restriction enzymes (Promega), and the gel was purified using GenElute™ Gel Extraction Kit (Sigma). PCR primers for mouse *Pax4* were designed with 15 bp extensions that are complementary to the ends of the pPB-tetO-MCS-IRES-mCherry linearised vector (Pax4 F: 5' - CAA AGA ATT CCT CGA ATG CAG CAG GAC GGA CT - 3′, Pax4 R: 5' - AGG CCA TGG CAC TAG TTA TGG CCA GTT TGA GCA ATG GGT TGA - 3′). The 15 bp extension was required for directional cloning using the In-Fusion HD cloning kit (Clonetech). From this point on, the manufacturer's instructions were followed. Pax4 was amplified using as template cDNA generated from mouse intestinal organoids. The generated plasmid was named pPB-tetO-*Pax4*-IRES-mCherry. The simultaneous co-transfection of three different plasmids is required for the generation of inducible overexpressing Pax4 human terminal ileal organoids. These plasmids are pPB-tetO-*Pax4*-IRES-mCherry, pPB-CAG-rtTA-IRES-Hygro and pCAG-PBase plasmid. For electroporation of the three plasmids into human terminal ileal cells, we followed the protocol from Fujii et al. [35]. DNA was transfected at 7.2 μg for the two piggyBac vectors, and at 5 μg for the transposase vector. Five days post-electroporation, cells were selected with 100 μg/mL hygromycin (Cambridge Bioscience). Gene expression was induced using 1 μg/mL of Doxycycline (Cambridge Bioscience).

2.14. Statistics

For cell counting experiments, "n" represents the number of individual organoids assessed. For RNA experiments, "n" represents the number of biological replicates. All data are presented as mean ± standard error of the mean (SEM), except violin plots, in which data are presented as median and quartiles. Each "n" is presented as a dot in graphs. Relevant tests are described in figure legends. All statistical analyses were performed using Graph Pad Prism Version 8.1.2 (GraphPad Software) for Windows or Mac except for RNA-seq, for which statistics were calculated using Seurat.

3. RESULTS

3.1. ISX-9 increases the expression of transcription factors associated with EEC differentiation

ISX-9 increases the expression of *NeuroD1* and induces differentiation of neuronal [27], cardiac [36] and islet endocrine progenitors [28]. We wondered if these properties could be harnessed to manipulate gut endocrine differentiation. Mouse small intestinal organoids exposed to increasing doses of ISX-9 (48-h treatment) had increased expression of transcription factors known to be important for endocrine specification (Figure 1A—F). As expected, ISX-9 increased *NeuroD1*, mimicking its role in other tissues (Figure 1A). Interestingly, *Ngn3*, a transcription factor usually associated with the earliest identifiable endocrine progenitor cell [37] and thought of being upstream of *NeuroD1*, was also increased (Figure 1B). Other downstream TFs were differentially affected by ISX-9, with *Pax4* being increased and *Arx* being unaffected (Figure 1C,D). *Atoh1* expression was inhibited at 40 and 80 μM, but there was little effect on *Hes1* expression at any dose, an indirect measure of Notch signalling (Figure 1E,F). Notch and *Atoh1* control the gate between the secretory and absorptive lineages [37]. These data suggest that ISX-9 may act downstream of this node and could favour the differentiation of specific EEC subsets based on its differential effects on *Pax4* and *Arx*.

We chose to use the 40 μM dose in further experiments, since at higher doses ISX-9 strongly inhibited *Atoh1* and did not significantly increase *NeuroD1*. To explore the effect of ISX-9 on gut epithelial homeostasis and EEC specification, we designed the following protocol. After passage, intestinal organoid cultures were maintained in stem cell growth media (WENR) for 3 days to create a stem cell enriched baseline. We then switched to differentiation media (ENR) and exposed cultures to ISX-9 for up to 4 days, which is the previously reported timeframe for maturation of EECs in intestinal organoids [38]. ISX-9 increased the expression of *Ngn3* and *NeuroD1* at 24, 48 and 96 h but only increased chromogranin A *(Chga)*, a gene selectively expressed in terminal-differentiated EECs [8], at 96 h (Figure 1G—I). This finding was highly reflective of the known differentiation trajectory of the EEC lineage. We next refined our paradigm to consist of a 48-

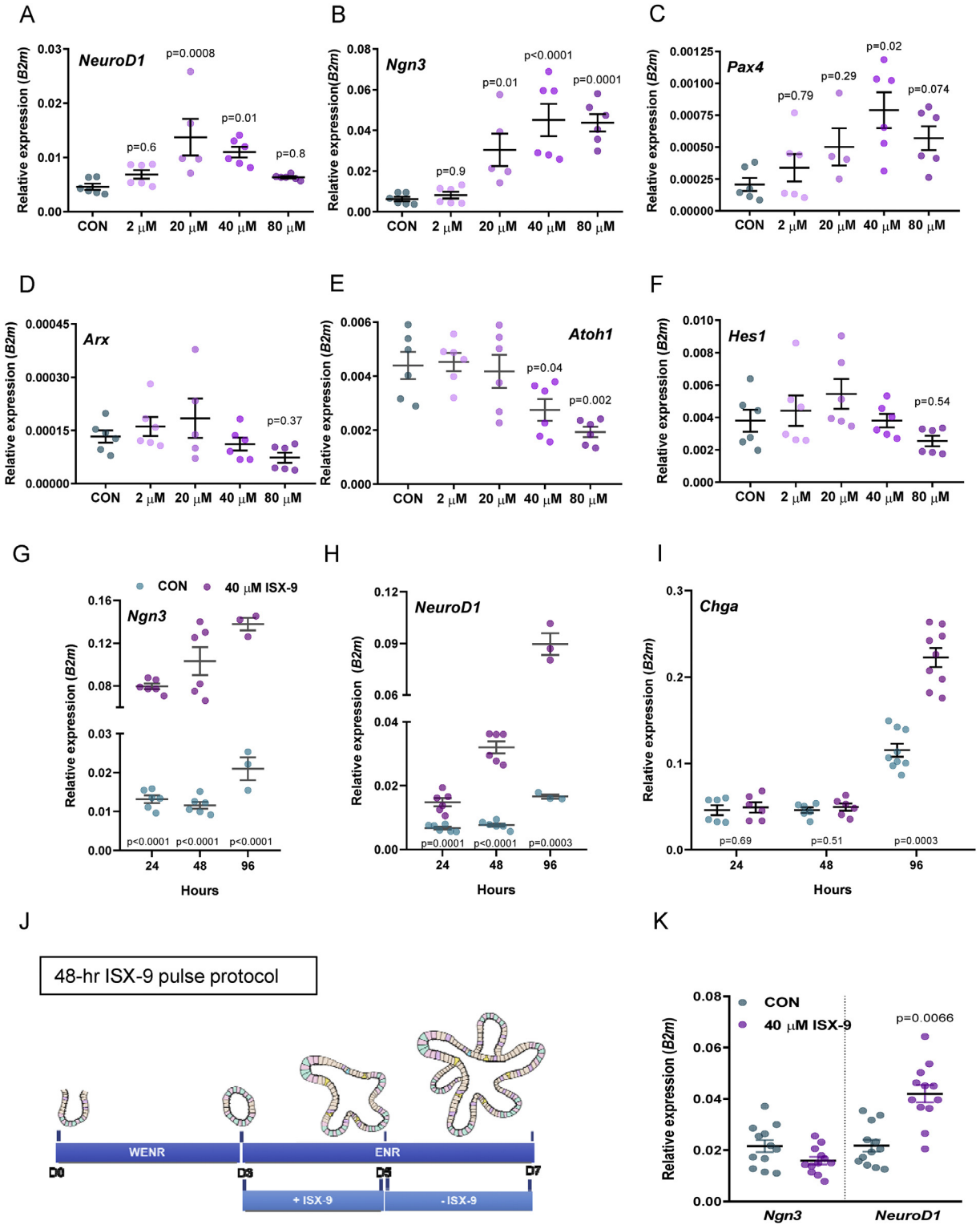

Figure 1: Effects of ISX-9 on the expression of transcription factors associated with EEC differentiation. (A–F) Expression of *NeuroD1* (A), *Ngn3* (B), *Pax4* (C), *Arx* (D), *Atoh1* (E) and *Hes1* (F) in mouse intestinal organoids cultured in the presence of increasing doses of ISX-9 (2–80 μM) for 48 h. (G–I) Expression of *Ngn3* (G), *NeuroD1* (H) and *ChgA* (I) in mouse organoids after 24, 48s and 96 h of continuous exposure to 40 μM ISX-9. (J) Schematic diagram explaining our experimental paradigm (K) Expression of *Ngn3* and *NeuroD1* in mouse intestinal organoids following our experimental paradigm. Data are represented as mean ± SEM. One-way ANOVA with Dunnett post-hoc test (A–F), unpaired two-tailed Student t test (G-I, K).

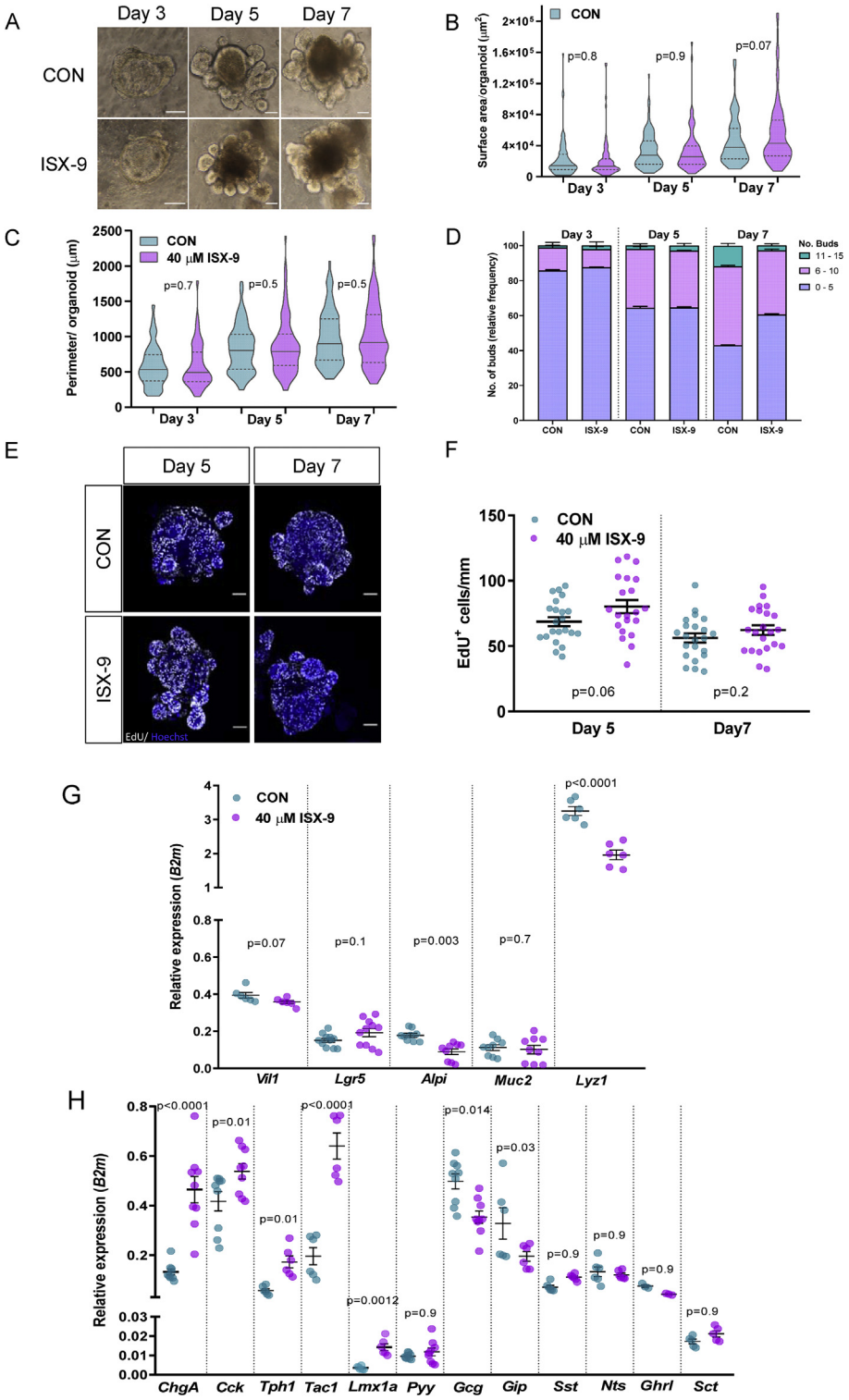

Figure 2: ISX-9 does not affect mouse intestinal organoid growth and specifically enriches markers of EC cells. (A) Representative brightfield images of mouse small intestinal organoids following the 48-hour ISX-9 pulse protocol. Surface area (B), perimeter (C) and number of buds (D) per control and treated organoids (n = 98). (E–F) Proliferating cells in control and ISX-9-treated organoids were visualised by the incorporation of 5-ethynyl-2′-deoxyuridine (EdU) (white) and counterstained with Hoechst (blue) (E). The number of Edu^{+} cells were counted for control and ISX-9-treated organoids on day 5 (at the end of 48-h ISX-9 treatment) and on day 7 (48 h after removal of ISX-9) (F). (G–H) qPCR analysis of lineage markers (G) and enteroendocrine-specific markers (H) in control and 48-hour ISX-9 pulse-treated organoids. Brightfield images are shown as one middle plain field of the organoid. Immunofluorescence images are shown as maximum intensity projections of a z-stack through the organoid. Scale bar: 50 μm. Data are represented as mean ± SEM, except in violin plots, where data are presented as median and quartiles. Unpaired two-tailed Student t test (B, C, F), one way-ANOVA with the Holms-Sidak multiple comparisons post-hoc test (G and H). The Kruskal–Wallis test with the Dunn post-hoc test (D).

hour pulse of ISX-9 at the beginning of the 4-day differentiation period, on day 3 of the protocol (Figure 1J). This removed a direct effect of ISX-9 as a confounding factor and ensured measurements made at the end of the protocol could be more easily attributed to altered cell fate. In this paradigm, *Ngn3* expression was unchanged, whereas *NeuroD1*, which is expressed in all early-to-late EEC subsets, remained elevated at 96 h, indicating that the ISX-9 pulse increased EEC specification in mouse intestinal organoids (Figure 1K).

3.2. ISX-9 specifically enriches markers of EC cells and does not affect organoid growth

Having established a paradigm in which ISX-9 appeared to increase EEC differentiation, there was a need to determine if this was authentic manipulation of cell fate or a consequence of increasing general organoid growth. We measured the morphological characteristics of organoids at different time points during our protocol: day 3 at baseline, day 5 immediately following the ISX-9 pulse, and day 7, the end of the differentiation period. There were no obvious differences between ISX-9-treated and control organoids in their general appearance or growth rates (Figure 2A). Equally, we found no difference between treatment and control in either surface area or perimeter of the organoids (Figure 2B,C). We noted a trend for a decrease in the proportion of very budded ISX-9-treated organoids (those with >5 buds) at day 7 (Figure 2D). This finding could suggest a decrease in stem cell proliferative capacity. However, in accordance with the surface area and perimeter observations, the number of EdU^+ cells (a marker of cells in S-phase and therefore undergoing proliferation) did not differ between treatments immediately post ISX-9 treatment or at the end of the study (Figure 2E,F). These results expand our evidence that ISX-9 alters cell fate and increases the EEC lineage independently of organoid growth.

To probe the effect of ISX-9 on epithelial lineages and EEC subset differentiation, we analysed the expression of markers of individual cell types at the end of the differentiation protocol. In line with the growth data, the expression of villin *(Vil1)*, a general epithelial marker, was unaltered between groups, as was the marker for goblet cells, mucin 2 (*Muc2*) (Figure 2G). The marker for stem cells, leucine-rich repeat-containing G-protein-coupled receptor 5 (*Lgr5*), was slightly increased but not significantly, whereas the enterocyte marker, alkaline phosphatase (*Alpi*), and the Paneth cell marker, lysozyme (*Lyz1*), were significantly decreased (Figure 2G). Within the EEC lineage, ISX-9 increased markers of I cells (*Cck*) and EC cells [tachykinin precursor 1 (*Tac1*), tryptophan hydroxylase 1 (*Tph1*), chromogranin A (*ChgA*) and *Lmx1a*] (Figure 2H). TPH1 is the rate-limiting enzyme for peripheral serotonin (5-HT) production, and EC cells are the most numerous gut endocrine cell type, producing 90% of the body's peripheral serotonin [23]. Whereas, Lmx1a is a transcription factor essential for the production of TPH1 [23]. Expression of L cell markers were unchanged (*Pyy*) or decreased (*Gcg*), as was the marker for K cells (*Gip*) (Figure 2H). The markers for D cells (*Sst*), N Cells (*Nts*), X cells (*Ghrl*) and the promiscuous marker secretin (*Sct*) were all unchanged in response to ISX-9 (Figure 2H). Together, these data imply that ISX-9 specifically increases the EEC lineage and drives cells to be fated toward EC cells and *Cck*-expressing cells rather than other mature EEC subtypes.

3.3. ISX-9 increases *Ngn3* endocrine fated populations

To determine if we were observing specific alterations in EEC cell fate, we used lineage tracing, fluorescent activated cell sorting, single-cell RNA-seq and immunostaining. First, we generated small intestinal organoids from *Tg(Ngn3-RFP)* mice which mark the *Ngn3* progenitor pool with turbo RFP [30]. We saw a five-fold increase in the percentage of RFP^+ cells immediately after ISX-9 treatment, using flow cytometry, which corroborated our expression data (Figure 3A).

To uncover the effect of ISX-9 on sub-populations of $Ngn3^+$ cells and to attempt to identify its key regulatory mechanisms, we employed single cell RNA-seq on sorted RFP^+ cells immediately after the ISX-9 treatment. The unsupervised clustering of cells, using conserved markers between control and ISX-9 treated cells, identified nine clusters split into two major branches, endocrine and non-endocrine (Figure 3B,C). The endocrine lineage contained five clusters: early-*Ngn3* (Hi *Ngn3* and, *Sox4*), late-*Ngn3* (Hi *Ngn3*, *Cnot6l, Nkx2-2, Neurod1, Pax4* and *Runxlt1*), endocrine progenitor (*Tac1, Chgb, Hmgn3* and *Cited2*), EC (*Chga, Tph1, Lmx1a* and *Reg4*) and EEC (*Pyy, CCK, Gcg* and *Nts*) (Figure 3B, Suppl. Figure 1A). The EC and EEC clusters are consistent with recent reports of two major branches of endocrine development, one containing EC cells and the other containing peptidergic gut-hormone-producing cell types [24,39]. The non-endocrine branch consisted of four clusters. We designated one cluster as goblet progenitors because they exhibited strong goblet cell marker expression (e.g., *Spink4*, *Muc2* and *Tff3*) but also contained Paneth cell markers (e.g., *Lyz1* and *Defa24*). Two other clusters were identified as enterocyte progenitors on account of their expression of *Cftr* and *Krt19*; these clusters were distinguished from one another by one cluster expressing markers of proliferation (*Top2A* and *Mik67)* (Figure 3B, Suppl. Figure 1A). An additional hard-to-define cluster was designated as non-endocrine progenitors (*Fryl, Plac8, Stat1* and *Grk4*). Examination of the cluster distributions by treatment showed an increased proportion of cells in the developmentally early endocrine clusters, Early-*Ngn3* and Late-*Ngn3,* in response to ISX-9 (Figure 3D and Suppl. Figure 1B,E). Coincidentally, there was a decrease in the number of cells in the non-endocrine branch (Figure 3D and Suppl. Figure 1B). Given the increased expression of EC markers and the I-cell marker *Cck* in our original experiments, ISX-9 plausibly biases endocrine lineage cells toward these pedigrees. However, a closer examination of *Cck* expression demonstrated a low level of promiscuous expression throughout the endocrine branch in contrast to other classical gut hormones (*Pyy, Ghrl, Fabp5* and *Gcg*), which were restricted to the EEC cluster (Figure 3B and Suppl. Figure 1C). We explored possible mechanisms of EC bias by examining TFs known to regulate endocrine differentiation. ISX-9 increased the expression of *Ngn3* and *NeuroD1* in the late-Ngn3 cluster, but notably increased both the expression and percentage of cells expressing *Pax4* in this cluster (Figure 3E—G and Suppl. Figure 1E). Strikingly, ISX-9 increased the expression of genes associated with EC progenitor bias (*Rfx6, Fev, Prdm16* and Hmgn3) whilst decreasing genes associated with EEC bias (*Isl1, Arx* and *Cdkn1a*) (Figure 3E,F, Suppl. Figure 1D) [24].

Together these data suggest that ISX-9 increases the flux of cells through the endocrine branch in part at the expense of the non-endocrine route and increases the expression of an EC-biased genetic program in these endocrine progenitors. In addition, the powerful increase in both *Pax4* expression and the percentage of $Pax4^+$ cells in the late Ngn3 cluster highlights a potentially novel mechanism of early EC bias in response to ISX-9 (Figure 3E,G).

3.4. ISX-9 increases the Ngn3 lineage and enriches it with functional EC cells

Next, we took advantage of a *Tg(Ngn3-cre)C1Able/J::R26-loxSTOPlox-tdRFP* (*Ngn3-Cre-RFP*) reporter transgenic line to examine the whole endocrine lineage including the $Ngn3^+$ progenitor pool and all daughter cell types (Figure 4A) [31,40]. A 48-hour ISX-9 pulse increased the percentage of $tdRFP^+$ cells analysed by flow cytometry

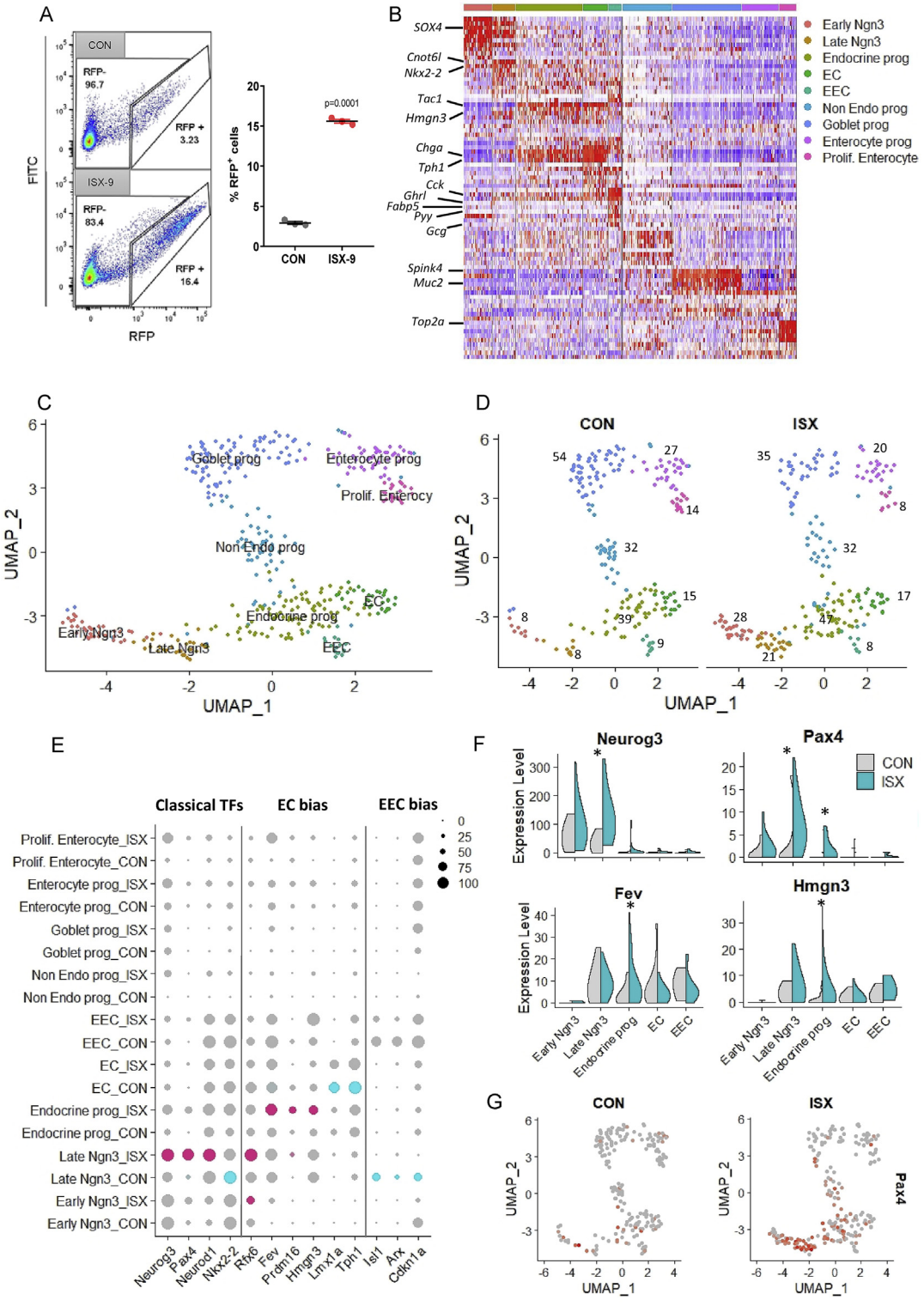

Figure 3: ISX-9 increases *Ngn3* endocrine fated populations with a bias toward EC cells. Intestinal organoids derived from Ngn3-RFP had a 48-hour ISX-9 treatment or were left untreated. Immediately after treatment, fluorescently labelled cells were sorted for further analysis. (A) Flow cytometric scatter plots of control vs. treatment and percentage of RFPþ cells recovered (unpaired two-tailed Student t test). (B) Combined expression heatmap of top 10 conserved marker genes between control and treated cells for each cluster. (C) UMAP projection depicting clusters identified by conserved marker expression between control and treatment. (D) UMAP projection of clusters split by treatment. (E) Dot plot of transcription factors known to influence endocrine and EC cell fate comparing control versus ISX treatment across clusters. Size of dot represents the percentage of cells expressing the gene of interest within cluster. The colour intensity represents average expression level: the more intense the colour (blue CON, pink ISX), the greater the average expression. (F) Violin plots of average Neurog3, Pax4, Fev, and Hmgn3 expression by cluster and treatment. (G) UMAP projections of Pax4 expression comparing control vs. treatment. * = adj. p value for Neurog3 (0.01), Pax4 (late Ngn3 = 0.04, endocrine prog = 0.0015), Fev (0.015) and Hmgn3 (0.03).

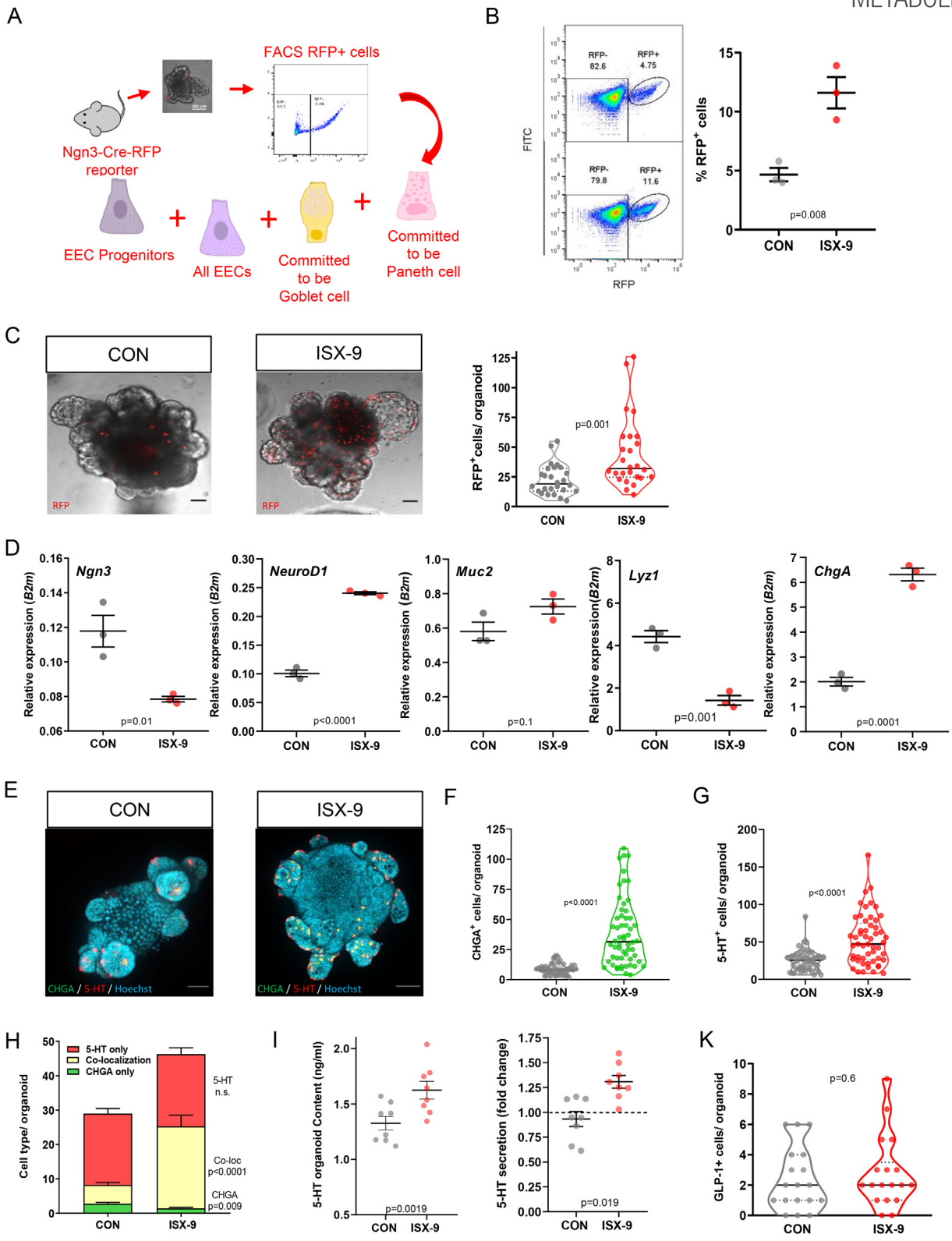

Figure 4: ISX-9 increases the number of Ngn3^{+} endocrine progenitors and enriches mouse intestinal organoids with functional enterochromaffin cells. (A) Experimental design schematic. The number of RFP^{+} cells in Ngn3-Cre-RFP mouse intestinal organoids treated with a 48-hour ISX-9 pulse was increased compared with controls as shown by flow cytometric analysis (B) and by counting from live-imaging (n = 26) (C). (D) Expression levels of *Ngn3*, *NeuroD1*, *Muc2*, *Lyz1* and *ChgA* in RFP^{+} cells sorted from Ngn3-Cre-RFP mouse intestinal organoids. (E) Confocal images of double immunofluorescent staining of for CHGA (green) and 5-HT (red). (F–H) Quantification of singly labelled CHGA+ and 5-HT + cells (F and G), and cells that co-localised these antigens (H) (n = 53–58). (I) 5-HT content and release measured by enzyme-linked immunosorbent assay (ELISA) (n = 8). (K) Quantification of GLP-1^{+} cells (n = 18). Live-cell images are shown as one middle plain for brightfield and as maximum intensity projections of a z-stack for RFP. Immunofluorescence images are shown as maximum intensity projections of a z-stack. Scale bar: 50 μm. All data are represented as mean ± SEM, except in violin plots, where data are presented as median and quartiles. Unpaired two-tailed Student t test.

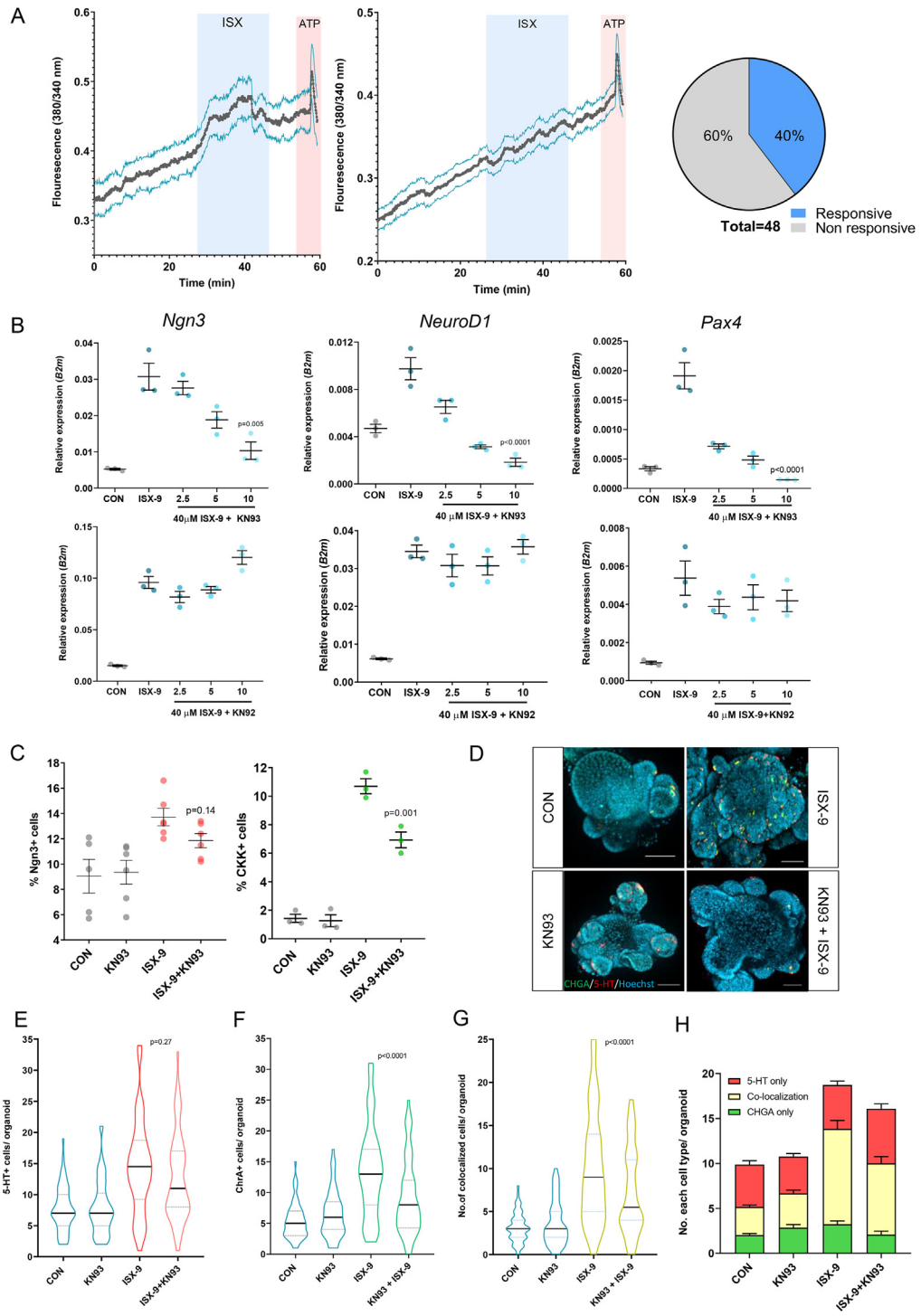

Figure 5: Enterochromaffin cell enrichment is partly dependent on ISX-9-induced calcium signalling. (A) Live-cell imaging of intracellular calcium in mouse small intestinal organoids using fluorescent indicator Fura-2 AM. Representative temporal plots of $[Ca^{2+}]i$ changes are shown, expressed as F340/380, in responsive cells (left) and non-responsive cells (middle) upon exposure to 40 μM ISX-9, followed by 100 μM ATP. Pie chart (right) shows the proportions of cells responsive to 40 μM ISX-9 (two individual experiments). (B) Expression of *Ngn3*, *NeuroD1* and *Pax4* in mouse organoids after 48-hour exposure to 40 μM ISX-9 in the presence of increasing doses of KN93 (top panel) or KN92 (bottom panel). (C) Flow cytometric analysis of $Ngn3^+$ and CCK^+ cells from Ngn3-Cre-RFP and CCK-Cre-eYFP organoids, respectively, in the presence or absence of ISX-9, KN93 or combination of both, for 48 h. Data are representative of a single experiment with n = 3. (D) Images of double immunofluorescent staining of control and ISX-9, KN93, or combination of both treated organoids for CHGA (green) and 5-HT (red). (E–G) Quantification of total 5-HT^+ (E), total $CHGA^+$ cells (F), and cells that co-localised these antigens (G) in control and ISX-9- and KN93-treated organoids. (H) Quantification of singly labelled 5-HT^+, $CHGA^+$ cells and co-localised cells (n = 59–64). All confocal images are shown as maximum intensity projection of a z-stack. Scale bar: 50 μm. Data are represented as mean ± SEM, except in violin plots where data are presented as median and quartiles. One-way ANOVA with the Sidak post-hoc test. (H) CHGA - CON vs ISX-9, $p = 0.1574$; ISX-9 vs ISX-9+KN93, $p = 0.3217$; CON vs ISX-9+KN93, $p = 0.9714$. 5-HT - CON vs ISX-9, $p = 0.9878$; ISX-9 vs ISX-9+KN93, $p = 0.1733$; CON vs ISX-9+KN93, $p = 0.0913$. Co-localisation – CON vs ISX-9, $p < 0.0001$; ISX-9 vs ISX-9+KN93, $p = 0.0118$; CON vs ISX-9+KN93, $p < 0.0001$.

(Figure 4B) and doubled the number of tdRFP + cells per organoid (Figure 4C). Expression analysis of sorted populations confirmed our earlier findings, with *Ngn3* and *NeuroD1* being increased immediately after 48-hour ISX-9 treatment whilst *Lyz1* (Paneth) was decreased and *Muc2* (goblet) and *ChgA* (EC cell) were unaltered (Suppl. Figure 2A). Forty-eight hours later, after removal of ISX-9, *Ngn3* was downregulated, *Muc2* was unchanged, *Lyz1* remained reduced, *NeuroD1* remained elevated and, as expected, *ChgA* was three-fold increased (Figure 4D), providing evidence that ISX-9 increases the endocrine progenitor pool and biases a proportion of these cells to become specific EC cells.

To further substantiate the expression data and demonstrate the programming of specific EEC subsets, we generated organoids from a *CCK-iCre*::*R26-loxSTOPlox-eYFP* reporter mouse (*CCK-Cre-eYFP*) [32,41]. ISX-9 increased the number of eYFP$^+$ cells per organoid by almost three-fold (Suppl. Figure 2B—C) and produced a similar increase in the percentage of eYFP$^+$ cells by flow cytometry analysis (Suppl. Figure 2D). In lieu of the availability of reporter mice for either chromogranin A or serotonin, we used immunocytochemistry to measure the effect of ISX-9 on the EC cell lineage. Double staining of whole organoids showed three cell populations: singly labelled 5-HT$^+$ and CHGA$^+$ cells, and cells that co-localised these antigens (Figure 4E). ISX-9 increased the total number of 5-HT$^+$ cells by two-fold and CHGA$^+$ cells by four-fold (Figure 4F,G). Analysis of the proportion of single versus co-localised cells showed the increase to be driven mainly by cells expressing both 5-HT and CHGA, which are likely endocrine EC cells (Figure 4H). ISX-9 increased organoid 5-HT content, and these newly generated cells were functional, releasing measurable 5-HT in response to stimulus (Figure 4I). ISX-9 did not alter GLP-1$^+$ immunofluorescent cell number (Figure 4K) despite *Gcg* expression being reduced, underpinning the selectivity of ISX-9's effect.

3.5. Enterochromaffin cell enrichment is partly dependent on ISX-9-induced calcium signalling

Mechanistically, ISX-9 promotes neuronal differentiation by stimulating intracellular calcium signalling [27]. Thus, it seemed logical to consider if this was also true of ISX-9's actions on EEC differentiation. To investigate this, we used calcium fluorometry in Fura-2 AM-loaded mouse organoids. ISX-9 induced a long and slow (approx. 15 min) increase in mean basal-to-peak calcium response in 40% of cells examined (Figure 5A and Suppl. Figure 3A—C). All cells including those that did not respond to ISX-9 produced the expected fast spike in calcium following administration of the positive control ATP (Figure 5A). Positionally, responders were never found at the base of the crypt buds, where Lgr5$^+$ stem cells reside (Suppl. Figure 3D—F).

In neuronal progenitors, ISX-9 increases calcium from both extra- and intracellular calcium sources [27]. We therefore chose to pharmacologically block ISX-9—induced calcium responses in organoids using the calcium calmodulin kinase II enzyme inhibitor KN93. CamKII is an important intracellular calcium signalling node. Interestingly, our single cell data demonstrated that the majority of *Camk2b*-expressing cells were restricted to the late Ngn3 and endocrine progenitor cell populations and showed a high degree of co-localisation with *Pax4*, particularly in the late Ngn3 progenitors (Suppl. Figure 3G). When given in conjunction with ISX-9, KN93 dose-dependently inhibited induction of *Ngn3*, *NeuroD1* and *Pax4*, whereas KN93's inactive analogue, KN92, did not (Figure 5B). Blocking CamKII signalling decreased the effect of ISX-9 on EEC differentiation. The expansion of *Ngn3*$^+$ and *Cck*$^+$ cells was decreased by approximately 30%—40% when KN93 was present (Figure 5C). KN92 did not affect the expansion of *Cck*$^+$ cells driven by ISX-9 (Suppl. Figure 3H). KN93 also attenuated the increase in total CHGA$^+$ cells by 50% and mildly but not significantly decreased the total number of 5-HT$^+$ cells (Figure 5D—H). As expected, KN93 had little effect on the singly labelled populations of 5-HT$^+$ and CHGA$^+$ (Figure 5E,F), but inhibited ISX-9-induced expansion of the co-localised population representing endocrine EC cells (Figure 5G,H). These data show that ISX-9 manipulates EEC differentiation in part by producing a calcium signal, likely in a population of early endocrine destined progenitors.

3.6. Enterochromaffin cell enrichment is replicated in human terminal ileal organoids

Historically, our understanding of mouse EEC differentiation has been based on knockout and lineage tracing *in vivo* studies, which were low throughput but provided key information regarding transcriptional regulation of EEC specification. The advent of organoid and single-cell technologies has rapidly expanded our knowledge in this area [24]. However, there is a deficit in our understanding of human epithelial EEC differentiation. Our mouse data identified ISX-9 as a useful tool to explore features of human EEC differentiation.

We began by validating a differentiation protocol in organoids generated from terminal ileal (TI) biopsies. Organoids were stimulated to differentiate by decreasing Wnt signalling for 7 days. This protocol led to decreased *LGR5* and *LYZ1* but increased *ALPI*, *VIL1* and *MUC2* (Suppl. Figure 4). As expected, we observed strong increases in the expression of EEC markers, *NGN3*, *NEUROD1*, *CHGA*, *TPH1, GCG*, *PYY*, *SST*, *GHRL* and *NTS*, suggesting a broad augmentation of the lineage. Interestingly, *CCK* and *TAC1* were not increased during the differentiation protocol (Suppl. Figure 4). Next, we designed an ISX-9 protocol for human TI that closely matched our mouse protocol. This consisted of a 3-day baseline period using stem cell media (WENRAS) followed by 7 days in differentiation media. A 48-hour ISX-9 pulse was delivered on day 6 (Figure 6A). The human TI transcriptional response was remarkably similar to that of the mouse. *NGN3, NEUROD1* and *PAX4* expression were increased after 48-hour exposure to ISX-9 (day 8) (Figure 6B). At the end of the differentiation protocol (day 10), ALPI and *LYZ1* expression were decreased, MUC2 was unchanged and LGR5 was increased (Figure 6C). Examination of endocrine markers following the same protocol showed that the response to ISX-9 in human intestinal organoids mirrored that of the mouse. *TAC1*, *TPH1*, *CHGA, LMX1A* and *CCK* were increased, suggesting enrichment for EC and Cck$^+$ cells, whereas markers of L cells (*PYY, GCG*), X cell (*GHRL*) and D cells (*SST*) were downregulated (Figure 6C,D). Immunofluorescent staining confirmed EC cell enrichment, driven mainly by an expansion of cells expressing both 5-HT$^+$ and CHGA$^+$ (Figure 6E—G). These new cells were functional, secreting 5-HT into the media following stimulation (Figure 6H).

Overall our data point to ISX-9 programming endocrine progenitors toward an EC cell fate, prompting us to speculate whether combining ISX-9 with known stimulators of the whole EEC lineage would amplify the enrichment of EC cells. To do this, we compared the EEC transcriptional response between ISX-9; a combination of NOTCH inhibition (iNotch) and MEK inhibition (iMEK); and all three together. These inhibitors have been shown to drive EEC differentiation by inducing stem cell quiescence [9]. ISX-9 and the iNotch, iMEK combination produced differential transcriptional responses. The inhibitor combination decreased *LGR5* and *LYZ1* expression and, as expected, increased *ALPI*, *MUC2*, *NGN3*, *NEUROD1*, *CHGA*, *TPH1* and *CCK* expression (Suppl. Figure 5). In comparison, the ISX-9 response was characterised by increased *LGR5* and decreased *LYZ1* and *ALPI*. ISX-9 was equally effective as iNotch and iMEK at increasing *NEUROD1* and *CCK*

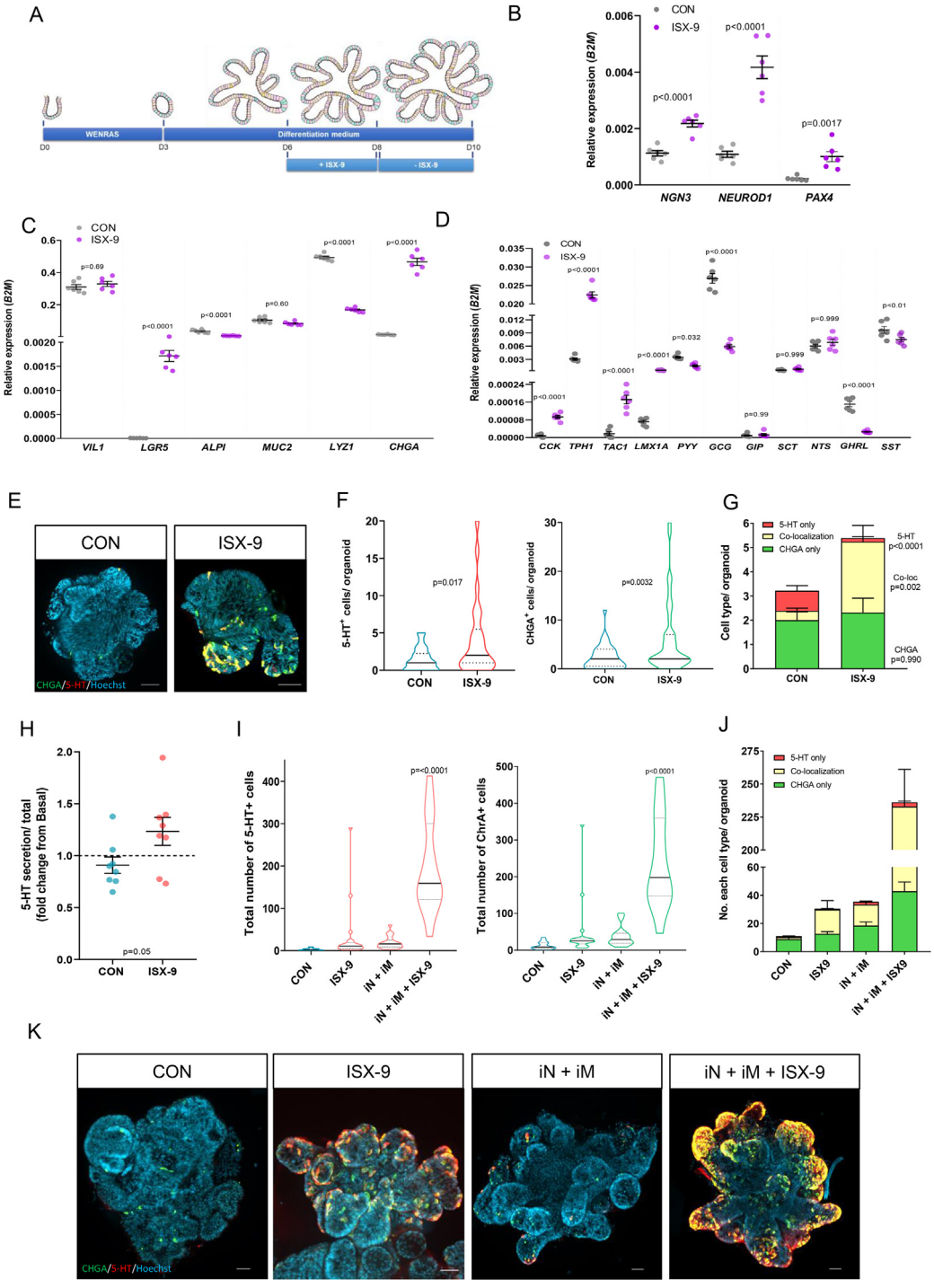

Figure 6: Effects of ISX-9 on human terminal ileal organoids. (A) Schematic diagram explaining the experimental paradigm of 48-hour ISX-9 pulse in human TI organoids. (B) Expression of *NGN3*, *NEUROD1* and *PAX4* in human TI organoids after 48-hour exposure to 40 μM ISX-9. qPCR analysis of lineage markers (C) and enteroendocrine-specific markers (D) in control and 48-hour ISX-9 pulse-treated human TI organoids. (E) Confocal images of double immunofluorescent staining of human TI organoids for CHGA (green) and 5-HT (red). (F) Quantification of total 5-HT$^+$ and total CHGA$^+$ cells. (G) Quantification of singly labelled 5-HT$^+$ cells and CHGA$^+$ cells and cells that co-localise these antigens human organoids (n = 25). (H) 5-HT release from human TI organoids as measured by ELISA. (I) Quantification of total 5-HT$^+$ and total CHGA$^+$ cells in control human TI organoids and in organoids treated with ISX-9, a combination of iNotch and iMEK, and all three together. (J) Quantification of singly labelled 5-HT$^+$ cells, CHGA$^+$ cells and cells that co-localised these antigens (n = 15–21). (K) Confocal images of double immunofluorescent staining of human TI organoids for CHGA (green) and 5-HT (red). All confocal images are shown as maximum intensity projections of a z-stack. Scale bar: 50 μm. Data are represented as mean ± SEM, except in violin plots where data are presented as median and quartiles. Unpaired two-tailed Student t test (F– H). One way-ANOVA with the Holms-Sidak multiple comparisons post-hoc test (B-D, I and J): (J) CHGA – CON vs ISX-9, p = 0.4473, ISX-9 vs iN + iM, pp = 0.1062; CON vs iN + iM, p = 0.0027; iN + iM vs iN + iM + ISX-9, p < 0.0001. 5-HT – CON vs ISX-9, p = 0.9216, ISX-9 vs iN + iM, pp = 0.0006; CON vs iN + iM, p = 0.0035; iN + iM vs iN + iM + ISX-9, p = 0.1079. Co-localisation – CON vs ISX-9, p = 0.0213, ISX-9 vs iN + iM, pp = 0.9683; CON vs iN + iM, p = 0.0597; iN + iM vs iN + iM + ISX-9, p < 0.0001.

but produced stronger increases in *NGN3*, *CHGA*, *TPH1* and *TAC1*, which was expected given its propensity for inducing EC cell enrichment. In combination, the two protocols powerfully and synergistically enriched organoids for markers of EC cells. Immunofluorescence staining confirmed a dramatic (100-fold) enrichment for endocrine EC cells (Figure 6I–K), providing further evidence that ISX-9 programmes early progenitors to become EC cells.

3.7. Overexpression of *Pax4* in human ileal organoids partially mimics the effect of ISX-9 on EEC differentiation

In our original experiments, *Ngn3*, *NeuroD1* and *Pax4* were identified as important transcription factors responding to ISX-9. Furthermore, at the single-cell level, our data highlighted a potential important role of *Pax4* in the late-Ngn3 and endocrine progenitors that may bias cells toward an EC cell fate. To explore the role of *Pax4*, we generated human TI organoids with a doxycycline (Dox)-inducible *Pax4* overexpressing transgene *Tg(tetO-mPax4-IRES-mCherry)::Tg(CMV-rtTA),* using a piggyBAC system (Figure 7A). We overexpressed mouse *Pax4*, which is 85% homologous to human *PAX4*, so that we could distinguish between endogenous and transgenic PAX4.

Dox treatment induced RFP expression within 24 h (Suppl. Figure 6A, Suppl. Movie 1), correlating with a 120-fold increase in mouse *Pax4* expression, further increasing by 500-fold after 48 h ($Pax4^{Hi}$) (Suppl. Figure 6B). Dox-inducible transgenes have been documented to be mildly leaky [42]. Indeed, our transgenic untreated organoids exhibited a low but significant level of *Pax4* expression (3-fold) ($Pax4^{Lo}$) compared with genetically identical wild-type controls maintained at the same passage. Fortuitously, the level of leaky expression was similar in magnitude to the induction by ISX-9 (Figure 5B), affording us the opportunity to examine *Pax4* gene dosage on EEC differentiation. We mirrored our ISX-9 protocol by using a 3-day baseline followed by a 7-day differentiation period and gave a pulse of Dox for 48 h on day 6. Selected transcriptional markers of epithelial cell types and EEC markers were analysed on day 10 (48 h after removal of Dox) (Figure 7B). In parallel with transgenic *Pax4* expression, endogenous *PAX4* expression was also increased, 3-fold in untreated and 100-fold in Dox-treated organoids, suggesting the existence of *Pax4* self-regulating pathways.

Supplementary video related to this article can be found at https://doi.org/10.1016/j.molmet.2020.01.012

$Pax4^{Lo}$ had no effect on *LGR5*, *LYZ1*, *VIL1* or *ALPI* expression but significantly increased *MUC2* expression compared with the wild-type control, suggesting increased goblet differentiation (Suppl. Figure 6C). *NGN3* and *NEUROD1* expression were both significantly increased as were *CHGA, TPH1* and *LMX1A* (EC cells), *CCK* (I cells), *PYY* (L cells), *NTS* (N cells), *GHRL* (G cells) and *SST* (D cells), whereas *GCG* (L cells), *TAC1* (early EC cells), *GIP* (K cells) were unchanged compared with wild type (Figure 7B and Suppl. Figure 7A), suggesting that low levels of *Pax4* overexpression induced selective specification of particular EEC subtypes including EC cells, partly mimicking the effect of ISX-9, but also inducing markers of N (*NTS*), D (*SST*) and X (*GHRL*) cells.

$Pax4^{Hi}$ significantly increased *LGR5*, *LYZ1* and *VIL1* whilst reducing *ALPI* and having no effect on *MUC2* (Suppl. Figure 6C). Unexpectedly, compared with Dox-negative transgenic controls, $Pax4^{Hi}$ did not enhance EEC specification, despite a 13-fold increase in *NGN3* expression (Figure 7B). In fact, the opposite was evident; all other EEC markers (*NEUROD1*, *CHGA*, *TPH1*, *LMX1A*, *NTS*, *PYY*, *CCK*, *GHRL*, *GCG*, *SST* and *GIP*) were either strongly decreased or undetectable (Figure 7B and Suppl. Figure 7A), except for *TAC1*, which was increased two-fold (Figure 7B).

This suggested EEC differentiation was stalled by high expression of *Pax4*. To investigate this further, we measured transcriptional markers on day 12 of our protocol, 96 h following removal of Dox. At this time point, $Pax4^{Hi}$ expression was decreased from 94-fold to a 3-fold induction (Figure 7C). Accordingly, endogenous *PAX4* induction was halved in the *Pax4* Hi group, demonstrating that *Pax4* expression was rapidly induced by Dox but was relatively slow to downregulate following Dox removal. Elevated *NGN3* expression was decreased from 13-fold to 2-fold, and *NEUROD1* was no longer suppressed (Figure 7C), which was associated with normalisation of *TAC1* expression and a disinhibition of EC cell markers (*CHGA, LMX1A* and *TPH1*) (Figure 7C). All other endocrine markers (*CCK, SST, NTS, GHRL, GCG, PYY* and *GIP*) remained supressed (Figure 7C and Suppl. Figure 7B). These data suggest that low levels of *Pax4* expression enhance EEC specification but high levels trap EECs in an early progenitor state with an EC cell bias. As *Pax4* expression normalises, endocrine differentiation proceeds with the appearance of EC cells. This finding helps explain ISX-9's effects on EC cell enrichment and suggests that the upregulation of *PAX4* and *TAC1* is important.

4. DISCUSSION

Enteroendocrine cells respond to diverse signals in the luminal environment including nutrients, microbial metabolites and pathogens. They play a central role in integrating these complex signals and altering physiology by modulating epithelial, immune, neuronal and hormonal functions. These features make the enteroendocrine system a potential target for treating multiple conditions and, notably, attention has focused on metabolic diseases [3]. An increasingly important feature of EECs is their plasticity, which hypothetically could be appropriated to alter their density and/or functional characteristics for therapeutic gain [43]. This is exemplified by two studies, which increased the secretory lineage *in vivo* using either a Notch or Rho-associated coiled-coil-containing protein kinase (ROCK) inhibitor [44,45]. The increased EEC density included GLP-1-producing L cells, promoting glucose control and decreasing hyperglycaemia in models of diabetes. The caveat to these proofs of principle studies is their broad effect across the secretory lineage. Targeting specific EEC differentiation pathways might be a more suitable approach but requires a deeper understanding of the regulatory networks controlling EEC specification, particularly in the human epithelium, which had been difficult to study before the advent of organoid technology.

We used ISX-9, a small molecule activator of *NeuroD1*, to further investigate EEC differentiation in mouse and human intestinal organoids. In the gut, *NeuroD1* is downstream of *Ngn3* in endocrine progenitors, and its deletion decreases the number of CCK and secretin cells in mice [46], potentially offering the opportunity to modulate specific EEC cell fates using ISX-9. Indeed, in our initial experiments, ISX-9 strongly increased classical TFs known to be key members of the regulator network controlling EEC differentiation (*Ngn3*, *NeuroD1* and *Pax4*), but did not affect *Arx*, suggesting specificity. An analysis of organoids derived from transgenic reporter mice or immunostained for serotonin showed that ISX-9 increased markers of endocrine progenitor development and demonstrated an enrichment of functional terminally differentiated EC cells. At single-cell resolution, we were able to corroborate the presence of two major developmental endocrine trajectories, peptidergic (gut hormone) versus enterochromaffin, and identify developmentally earlier endocrine clusters. An analysis of ISX-9 treated cells provided evidence of increased cells in the endocrine branch at the expense of the non-endocrine goblet/enterocyte

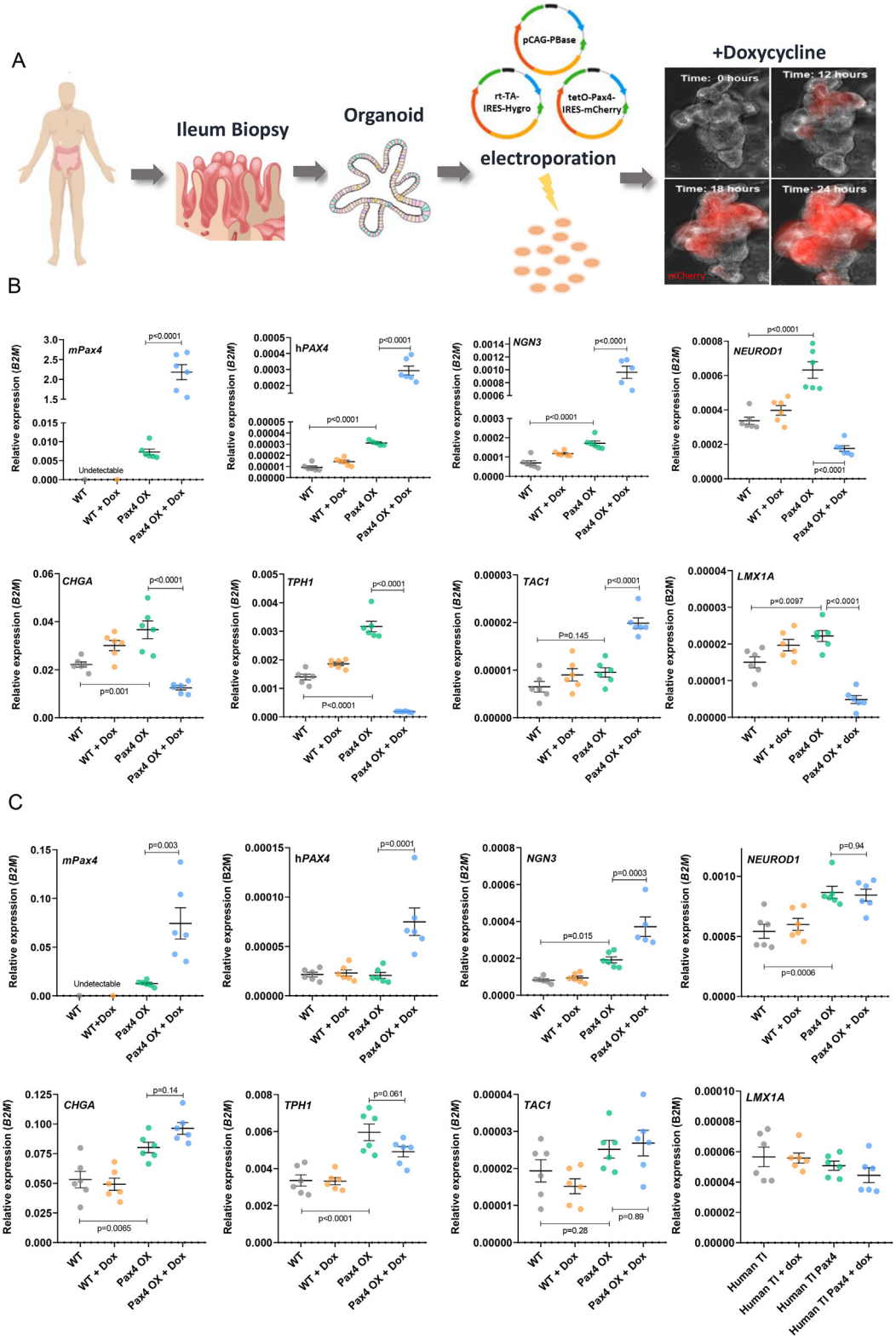

Figure 7: Overexpression of *Pax4* in human ileal organoids. (A) Schematic describing the production pipeline for the generation of *Pax4* overexpressing human ileal organoids. (B–C) Expression of mouse *Pax4*, human *PAX4*, *NGN3*, *NEUROD1* and EC cell markers (*CHGA, TPH1, TAC1* and *LMX1A*) in wild-type untreated organoids (WT), wild-type organoids induced for 48 h with 1 μg/mL doxycycline (WT + Dox), transgenic untreated *Pax4* human intestinal organoids (Pax4 OX) and transgenic *Pax4* human intestinal organoids induced for 48 h with 1 μg/mL doxycycline (Pax4 OX + Dox) that were collected for RNA extraction 48 h (B) or 96 h (C) after removal of Dox. One-way ANOVA with the Tukey post-hoc test.

lineages. A notable increase of Pax4 expression in the late-Ngn3 population coupled with an activation of a genetic program biased toward EC differentiation (*Rfx6, Fev, Prdm16* and Hmgn3) could explain the enrichment in functional EC cells. These actions were upstream of factors important for late EC cell differentiation or identity, *Lmx1a,* Chga and *Tph1,* which were increased at the final time point (i.e., 48 h after ISX-9 was removed). Importantly, this finding appeared to be a genuine manipulation of lineage fate and not an alteration in organoid growth. Equally, organoid proliferation and *Lgr5* expression were unaltered, in contrast to a previously published paradigm that promotes EEC lineage differentiation by inducing Lgr5 stem cell quiescence using NOTCH and MEK inhibitors [9].

The triggering of neuronal differentiation by ISX-9 is calcium dependent [27]. Similarly, its effect on the endocrine lineage was partly dependent on calcium signalling. Inhibition of the intracellular calcium signalling node, CamKII, attenuated EC and *Cck*$^{+}$ cell enrichment and blocked induction of *Ngn3*, *NeuroD1* and *Pax4* expression. This corresponds with recent data in Drosophila, showing that activation of the mechanosensitive receptor Piezo in a population of mid-gut endocrine progenitor cells increases EEC differentiation through cytosolic Ca^{2+} [47]. In mice, Piezo2 is found in a sub-population of EC cells that release serotonin in response to stretch [48]. Future work will be aimed at identifying in which cells ISX-9 stimulates calcium and whether calcium signalling is an important regulator of homeostatic endocrine differentiation in the gut.

Most data relating to EEC differentiation have been gathered in mice or using mouse tissues. Comparatively little is known about the networks controlling endocrine cell fate in the human gut epithelium, but they are assumed to be conserved to some degree, stemming largely from the study of patients with mutations in NGN3 who exhibit intractable malabsorptive diarrhoea due to loss of EECs and a handful of recent studies in organoids [49–51]. In these *in vitro* studies, a pulse of transgenic *NGN3* in iPSCs-derived human organoids mostly recapitulated the predicted endocrine repertoire [26]. The same transgenic construct has been deployed in organoids derived from tissue resident stem cells and similarly promoted EEC differentiation [52]. Our data shed further light on human EEC differentiation and its similarity to that of the mouse. Notably, ISX-9 produced identical effects on the EEC lineage between species. *NGN3*, *NEUROD1* and *PAX4* upregulation was associated with selective increases in *CCK*, *CHGA*, *TPH1, LMX1A* and *TAC1*. Whole organoid immunostaining confirmed enrichment for EC cells double positive for 5-HT and CHGA, and these cells functionally released 5-HT. Our data have several implications; they highlight how similar EEC specification is between the mouse and humans and that ISX-9 alone or in combination with iNotch and iMEK can be used to enrich human organoids with EC cells allowing functional exploration of these rare and difficult-to-study cells. EC cells modulate GI motility, bone formation, hepatic gluconeogenesis, thermogenesis, insulin resistance and regulation of fat mass [53]. Understanding how these cells function in humans has important implications.

Our data highlighted the potential importance of *Pax4*, and its induction in the late Ngn3 population seemed to offer a developmentally early mechanistic explanation for EC cell enrichment by ISX-9. However, low level constitutive expression produced a generalised increase in EEC lineage markers, although notable exceptions were *GCG* and *GIP*. We also observed a surprising and powerful upregulation of *NGN3*, suggesting reciprocal regulation between *PAX4* and *NGN3*. The upregulation of *MUC2* and *LYZ1* might also be explained by this *NGN3* upregulation, as 15% of goblet and 40% of Paneth cells are derived from Ngn3 progenitors [40]. Strikingly, induction of high levels of *Pax4* expression completely inhibited endocrine differentiation, trapping EEC differentiation at an early stage. Unexpectedly, induced transgenic *Pax4* was persistent, remaining upregulated by 3-fold 96 h after doxycycline removal, although this was reduced from a peak induction of 94-fold. Interestingly, at this time point, all markers of peptidergic EECs (*CCK, SST, NTS*, *GHRL*, GCG and PYY) remained supressed, but markers of mature EC cells (*LMX1A*, *CHGA and TPH1*) were now disinhibited, and *TAC1*, an early EC cell marker, was no longer upregulated. We drew several conclusions from these findings. First, our data are consistent with the existence of two major lineages of EECs in humans, as recently described in the mouse and corroborated by our single cell data [24,54]. One lineage gives rise to an early-appearing EC cell population and the other to peptidergic-producing cells, which generally appear later than EC cells. Second, *PAX4*, as in the mouse, is upstream of *NEUROD1* and likely marks an early endocrine progenitor cell. Third, understanding the network of TFs controlling EEC differentiation is complicated by their promiscuity and the need to appreciate the timing and level of expression. Finally, it seems plausible that ISX-9 enriches the ECC lineage in part by its effects on *PAX4* expression, which may represent an increase in the endocrine pool biased toward an EC cell fate.

Finally, our data add to a handful of studies suggesting that small molecules could be found to selectively control EEC cell fate/specification with a view to treat various clinical conditions. However, our data also highlight the difficulties this approach faces. Understanding to what degree the targeted lineage creates a deficit in another and whether this induces unwanted physiological effects is of key importance. This seems a likely event when intervening downstream of *NGN3*, where one EEC type may be enriched at the expense of another. This situation could be mitigated by combining selective EEC targeting with a more generalised EEC lineage activator. Realising this potential will require a much deeper understanding of human EEC lineage specification aided by the organoid platform.

AUTHOR CONTRIBUTIONS

A. T. and P. F. P. helped in the design of experiments, collected data and contributed to the writing of the manuscript. P.P and B.H.H provided human biopsies for the isolation of crypts. G. A. B. wrote the manuscript and managed the project.

CONFLICT OF INTERESTS

None declared.

ACKNOWLEDGEMENTS

For providing us with intestinal tissues from transgenic animals for the generation of small intestinal organoids we would like to thank Prof Anne Grappin-Botton (Neurog3-RFP mice), Dr Mathieu Latreille (*Tg(Neurog3-cre)C1Able/J*::*R26-loxSTOPlox-tdRFP* mice) and Dr Giuseppe D'Agostino (*CCK-iCre*::*R26-loxSTOPlox-eYFP* mice). We would also like to thank Dr Calvin Kuo and Dr Hans Clever for providing us with R-Sponding1-producing cell line and L-Wnt3A cells, respectively, and Dr Bon-Kyoung Koo for supplying the piggyBAC system for the generation of doxycycline induced Pax4/RFP overexpressing human ileal organoids. We would like to thank the staff in the Nikon Imaging Centre and in BRC Flow cytometry core at King's College London for all their help. This study was supported by grants awarded by European Foundation for the Study of Diabetes (EFSD) and Juvenile Diabetes Research Foundation (JDFR). PFP was funded as part of the Medical Research Council (MRC) Doctoral Training Partnership Programme, 2016 cohort (grant code: ST10262).

APPENDIX A. SUPPLEMENTARY DATA

Supplementary data to this article can be found online at https://doi.org/10.1016/j.molmet.2020.01.012.

REFERENCES

[1] Gehart, H., Clevers, H., 2019. Tales from the crypt: new insights into intestinal stem cells. Nature Reviews Gastroenterology & Hepatology 16(1):19—34.

[2] Gribble, F.M., Reimann, F., 2016. Enteroendocrine cells: chemosensors in the intestinal epithelium. Annual Review of Physiology 78:277—299.

[3] Sam, A.H., et al., 2012. The role of the gut/brain axis in modulating food intake. Neuropharmacology 63(1):46—56.

[4] Melvin, A., le Roux, C.W., Docherty, N.G., 2016. The gut as an endocrine organ: role in the regulation of food intake and body weight. Current Atherosclerosis Reports 18(8):49.

[5] Adriaenssens, A., et al., 2015. A transcriptome-led exploration of molecular mechanisms regulating somatostatin-producing D-cells in the gastric epithelium. Endocrinology 156(11):3924—3936.

[6] Habib, A.M., et al., 2012. Overlap of endocrine hormone expression in the mouse intestine revealed by transcriptional profiling and flow cytometry. Endocrinology 153(7):3054—3065.

[7] Knudsen, L.A., et al., 2015. The MicroRNA repertoire in enteroendocrine cells: identification of miR-375 as a potential regulator of the enteroendocrine lineage. Endocrinology 156(11):3971—3983.

[8] Engelstoft, M.S., et al., 2015. Research resource: a chromogranin A reporter for serotonin and histamine secreting enteroendocrine cells. Molecular Endocrinology 29(11):1658—1671.

[9] Basak, O., et al., 2017. Induced quiescence of Lgr5+ stem cells in intestinal organoids enables differentiation of hormone-producing enteroendocrine cells. Cell Stem Cell 20(2):177—190 e4.

[10] Beumer, J., et al., 2018. Enteroendocrine cells switch hormone expression along the crypt-to-villus BMP signalling gradient. Nature Cell Biology 20(8):909—916.

[11] Zecchini, V., et al., 2005. Notch signaling regulates the differentiation of post-mitotic intestinal epithelial cells. Genes & Development 19(14):1686—1691.

[12] Stanger, B.Z., et al., 2005. Direct regulation of intestinal fate by Notch. Proceedings of the National Academy of Sciences of the United States of America 102(35):12443—12448.

[13] Fre, S., et al., 2005. Notch signals control the fate of immature progenitor cells in the intestine. Nature 435(7044):964—968.

[14] Jenny, M., et al., 2002. Neurogenin3 is differentially required for endocrine cell fate specification in the intestinal and gastric epithelium. The EMBO Journal 21(23):6338—6347.

[15] Lee, C.S., et al., 2002. Neurogenin 3 is essential for the proper specification of gastric enteroendocrine cells and the maintenance of gastric epithelial cell identity. Genes & Development 16(12):1488—1497.

[16] Gradwohl, G., et al., 2000. neurogenin3 is required for the development of the four endocrine cell lineages of the pancreas. Proceedings of the National Academy of Sciences of the United States of America 97(4):1607—1611.

[17] Mutoh, H., et al., 1997. The basic helix-loop-helix transcription factor BETA2/NeuroD is expressed in mammalian enteroendocrine cells and activates secretin gene expression. Proceedings of the National Academy of Sciences of the United States of America 94(8):3560—3564.

[18] Naya, F.J., et al., 1997. Diabetes, defective pancreatic morphogenesis, and abnormal enteroendocrine differentiation in BETA2/neuroD-deficient mice. Genes & Development 11(18):2323—2334.

[19] Mutoh, H., et al., 1998. The basic helix-loop-helix protein BETA2 interacts with p300 to coordinate differentiation of secretin-expressing enteroendocrine cells. Genes & Development 12(6):820—830.

[20] Desai, S., et al., 2008. Nkx2.2 regulates cell fate choice in the enteroendocrine cell lineages of the intestine. Developmental Biology 313(1):58—66.

[21] Beucher, A., et al., 2012. The homeodomain-containing transcription factors Arx and Pax4 control enteroendocrine subtype specification in mice. PloS One 7(5):e36449.

[22] Ye, D.Z., Kaestner, K.H., 2009. Foxa1 and Foxa2 control the differentiation of goblet and enteroendocrine L- and D-cells in mice. Gastroenterology 137(6):2052—2062.

[23] Gross, S., et al., 2016. The novel enterochromaffin marker Lmx1a regulates serotonin biosynthesis in enteroendocrine cell lineages downstream of Nkx2.2. Development 143(14):2616—2628.

[24] Gehart, H., et al., 2019. Identification of enteroendocrine regulators by real-time single-cell differentiation mapping. Cell 176(5):1158—1173 e16.

[25] Spence, J.R., et al., 2011. Directed differentiation of human pluripotent stem cells into intestinal tissue in vitro. Nature 470(7332):105—109.

[26] Sinagoga, K.L., et al., 2018. Deriving functional human enteroendocrine cells from pluripotent stem cells. Development 145(19).

[27] Schneider, J.W., et al., 2008. Small-molecule activation of neuronal cell fate. Nature Chemical Biology 4(7):408—410.

[28] Dioum, E.M., et al., 2011. A small molecule differentiation inducer increases insulin production by pancreatic beta cells. Proceedings of the National Academy of Sciences of the United States of America 108(51):20713—20718.

[29] Kalwat, M.A., et al., 2016. Isoxazole alters metabolites and gene expression, decreasing proliferation and promoting a neuroendocrine phenotype in beta-cells. ACS Chemical Biology 11(4):1128—1136.

[30] Kim, Y.H., et al., 2015. Cell cycle-dependent differentiation dynamics balances growth and endocrine differentiation in the pancreas. PLoS Biology 13(3):e1002111.

[31] Luche, H., et al., 2007. Faithful activation of an extra-bright red fluorescent protein in "knock-in" Cre-reporter mice ideally suited for lineage tracing studies. European Journal of Immunology 37(1):43—53.

[32] D'Agostino, G., et al., 2016. Appetite controlled by a cholecystokinin nucleus of the solitary tract to hypothalamus neurocircuit. Elife 5.

[33] Muraro, M.J., et al., 2016. A single-cell transcriptome atlas of the human pancreas. Cells and Systems 3(4):385—394 e3.

[34] Stuart, T., et al., 2019. Comprehensive integration of single-cell data. Cell 177(7):1888—1902 e21.

[35] Fujii, M., et al., 2015. Efficient genetic engineering of human intestinal organoids using electroporation. Nature Protocols 10(10):1474—1485.

[36] Sadek, H., et al., 2008. Cardiogenic small molecules that enhance myocardial repair by stem cells. Proceedings of the National Academy of Sciences of the United States of America 105(16):6063—6068.

[37] Li, H.J., et al., 2011. Basic helix-loop-helix transcription factors and enteroendocrine cell differentiation. Diabetes, Obesity and Metabolism 13(Suppl 1):5—12.

[38] Petersen, N., et al., 2014. Generation of L cells in mouse and human small intestine organoids. Diabetes 63(2):410—420.

[39] Piccand, J., et al., 2019. Rfx6 promotes the differentiation of peptide-secreting enteroendocrine cells while repressing genetic programs controlling serotonin production. Molecular Metabolism 29:24—39.

[40] Schonhoff, S.E., Giel-Moloney, M., Leiter, A.B., 2004. Neurogenin 3-expressing progenitor cells in the gastrointestinal tract differentiate into both endocrine and non-endocrine cell types. Developmental Biology 270(2):443—454.

[41] Flak, J.N., et al., 2014. Leptin-inhibited PBN neurons enhance responses to hypoglycemia in negative energy balance. Nature Neuroscience 17(12):1744—1750.

[42] Zhu, Z., et al., 2001. Use of the tetracycline-controlled transcriptional silencer (tTS) to eliminate transgene leak in inducible overexpression transgenic mice. Journal of Biological Chemistry 276(27):25222—25229.

[43] Tsakmaki, A., Pedro, F.P., Bewick, G.A., 2017. 3D intestinal organoids in metabolic research: virtual reality in a dish. Current Opinion in Pharmacology(37C):51—58.
[44] Petersen, N., et al., 2015. Targeting development of incretin-producing cells increases insulin secretion. Journal of Clinical Investigation 125(1):379—385.
[45] Petersen, N., et al., 2018. Inhibiting RHOA signaling in mice increases glucose tolerance and numbers of enteroendocrine and other secretory cells in the intestine. Gastroenterology 155(4):1164—1176 e2.
[46] Schonhoff, S.E., Giel-Moloney, M., Leiter, A.B., 2004. Minireview: development and differentiation of gut endocrine cells. Endocrinology 145(6):2639—2644.
[47] He, L., et al., 2018. Mechanical regulation of stem-cell differentiation by the stretch-activated Piezo channel. Nature 555(7694):103—106.
[48] Alcaino, C., et al., 2018. A population of gut epithelial enterochromaffin cells is mechanosensitive and requires Piezo2 to convert force into serotonin release. Proceedings of the National Academy of Sciences of the United States of America 115(32):E7632—E7641.
[49] Pinney, S.E., et al., 2011. Neonatal diabetes and congenital malabsorptive diarrhea attributable to a novel mutation in the human neurogenin-3 gene coding sequence. Journal of Clinical Endocrinology & Metabolism 96(7): 1960—1965.
[50] Rubio-Cabezas, O., et al., 2011. Permanent neonatal diabetes and enteric anendocrinosis associated with biallelic mutations in NEUROG3. Diabetes 60(4):1349—1353.
[51] German-Diaz, M., et al., 2017. A new case of congenital malabsorptive diarrhea and diabetes secondary to mutant neurogenin-3. Pediatrics 140(2).
[52] Chang-Graham, A.L., et al., 2019. Human intestinal enteroids with inducible neurogenin-3 expression as a novel model of gut hormone secretion. Molecular Cell Gastroenterology and Hepatology 8(2):209—229.
[53] Yabut, J.M., et al., 2019. Emerging roles for serotonin in regulating metabolism: new implications for an ancient molecule. Endocrine Reviews 40(4): 1092—1107.
[54] Julie Piccand, C.V., Blot, Florence, Meunier, Aline, Anthony, Beucher, Strasser, Perrine, Lund, Mari L., et al., 2019. Rfx6 promotes the differentiation of peptide-secreting enteroendocrine cells while repressing genetic programs controlling serotonin production. BioRxiv.

